ChemComm

COMMUNICATION

View Article Online
View Journal | View Issue

Cite this: *Chem. Commun.*, 2014, **50**, 11698

Received 23rd June 2014,
Accepted 15th August 2014

DOI: 10.1039/c4cc04754k

www.rsc.org/chemcomm

Dynamic response of ultrathin highly dense ZIF-8 nanofilms†

Joanna Cookney,[abc] Wojciech Ogieglo,[a] Pavel Hrabanek,[d] Ivo Vankelecom,[c] Vlastimil Fila[b] and Nieck E. Benes*[a]

Ultrathin ZIF-8 nanofilms are prepared by facile step-by-step dip coating. A critical withdrawal speed allows for films with a very uniform minimum thickness. The high refractive index of the films denotes the absence of mesopores. The dynamic response of the films to CO_2 exposure resembles behaviour observed for non-equilibrium organic polymers.

Metal–organic frameworks (MOFs) represent one of the fastest growing fields in materials chemistry. MOFs are porous hybrid organic–inorganic frameworks that retain properties of conventional inorganic materials but at the same time possess much lower densities than most organic systems. Due to their enormous structural and chemical diversity,[1,2] MOFs offer vast opportunities for development of technologically relevant and widely applicable materials.[3–6] Zeolitic imidazolate frameworks (ZIFs), a subclass of MOFs, consist of bivalent metal cations solely coordinated by nitrogen atoms of the imidazolate bridging ligand, forming microporous crystalline lattices. ZIFs have been recognized for their chemical and thermal stability, unusual for MOFs.[7,8] The prototypical ZIF-8 is synthesized *via* the assembly of tetrahedrally coordinated zinc ions (Zn^{2+}) and 2-methylimidazole (Hmim) organic linkers that form three-dimensional open structures with well-defined cavities (11.6 Å) that are accessible *via* small pore apertures (3.4 Å).[8] The exceptionally high thermal and chemical stability of ZIF-8,[9] combined with its regular microstructure, led to extensive investigations on ZIF-8 in the field of membrane science,[10–12] gas storage,[13,14] and catalysis.[15]

A rapidly growing interest in optical- and magnetic-based devices has further increased the attention towards the development of thin MOF films.[16–21] Nevertheless, reports on the synthesis of supported ZIF-8 thin films are relatively scarce.[22–26] The approaches employed to construct such thin films can be broadly categorized into two groups: step-by-step deposition and dip coating from colloidal solutions. The stepwise strategy consists of substrate immersion into a Zn^{2+} solution, washing with a solvent, dipping into an Hmim rich solution, and finally washing again. This procedure counts as a full growth cycle and its repetition results in the formation of thicker, well-intergrown crystalline films.[22,26] Growth from colloidal solutions gives the advantage of the precise control of crystal size, although the presence of interparticular voids[23] can significantly alter the sorption behaviour of the films. In some cases, surface modification favours development of oriented ZIF-8 nanolayers.[26] However, the synthesis of uniform, continuous and grain boundary free films still remains a challenge.

Here we present the synthesis of ultrathin ZIF-8 nanofilms by facile step-by-step dip coating, employing only a single growth cycle (Fig. 1a). In addition to their low and uniform thickness, the films are distinct in that they exhibit a very dense and homogenous morphology that is partly crystalline, and are accessible to small penetrants. Pivotal is the slow withdrawal speed u during coating that allows direct control of the film thickness.

Three regimes can be distinguished in Fig. 1b and c. The regime at lower withdrawal speeds ($u < 1$ mm s^{-1}) is known as the capillary regime and is governed by the combined effects of continuous capillary feeding and methanol evaporation. Decreasing u in the capillary regime results in an increased film thickness. At the lowest u of 0.1 mm s^{-1} a 217 ± 2.85 nm thick film was obtained. The regime at higher speeds ($u > 3$ mm s^{-1}) is known as draining regime. In this regime, gravity-induced viscous draining opposes solvent adhesion to the substrate, as described by the Landau–Levich model.[27] In the intermediate regime, the draining and capillary effects overlap and the fluid viscosity and the rate of solvent evaporation are interdependent. At a critical withdrawal speed of u_c = 1 mm s^{-1}, a minimum film thickness of 106 ± 0.74 nm is obtained. Similar trends of thickness *versus* coating velocity have been previously reported for the synthesis of sol–gel

[a] *Inorganic Membranes, Department of Science and Technology, Mesa+ Institute for Nanotechnology, University of Twente, P.O. Box 217, 7500 AE Enschede, The Netherlands. E-mail: n.e.benes@utwente.nl*
[b] *Department of Inorganic Technology, Institute of Chemical Technology Prague, Technicka 5, 16628 Prague 6, Czech Republic*
[c] *Centre for Surface Chemistry and Catalysis, KU Leuven, Kasteelpark Arenberg 23, 3001 Heverlee, Belgium*
[d] *J. Heyrovsky Institute of Physical Chemistry of the ASCR, v.v.i., Dolejskova 2155/3, 18223 Prague 8, Czech Republic*

† Electronic supplementary information (ESI) available: Synthesis procedure, characterization, estimation of the film porosity. See DOI: 10.1039/c4cc04754k

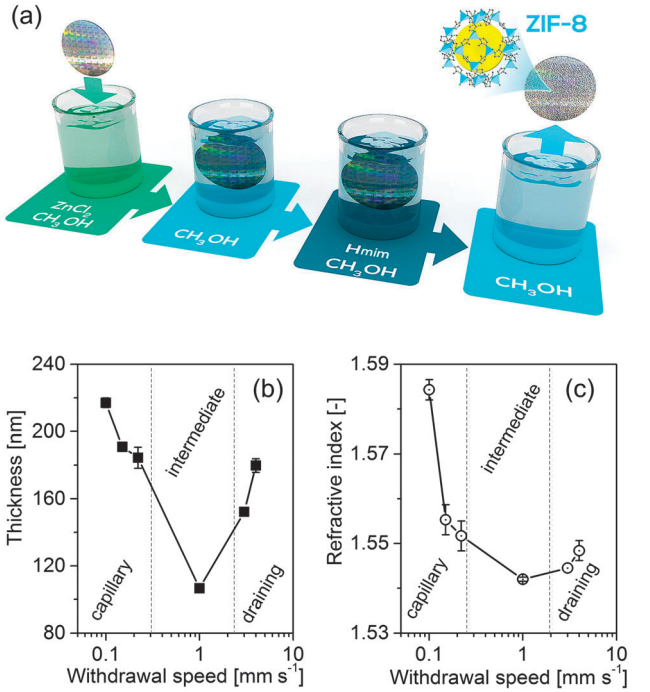

Fig. 1 (a) Illustration of step-by-step dip coating employed for the synthesis of ZIF-8 nanofilms; the growth cycle is only conducted once (b) film thickness dependency on the withdrawal speed, (c) refractive index as a function of withdrawal speed. The solid line is a guide to the eye, the position of the dotted lines is only indicative. The error bars illustrate the standard deviations determined from three spot measurements on each of the films, indicating the highest film uniformity at intermediate speed.

films[28] and for the development of ZIF-8 crystalline nanofilms from colloidal solution.[23]

The refractive index n of the films shows a strong dependency on the kinetics of deposition, with an overall trend resembling that of the thickness (Fig. 1c). In the capillary regime, n increases substantially with decreasing u. The highest value of the refractive index (n = 1.584, determined directly after dip-coating) is observed at the lowest withdrawal speed. This can be rationalized from the more pronounced capillary forces that develop upon solvent evaporation at lower withdrawal rates, resulting in a higher materials density and hence a higher refractive index. In the draining regime, the refractive index moderately increases with increasing withdrawal rate. In the intermediate region, a minimum value is observed, n = 1.542. The observed trends are in a reasonable agreement with the results reported by Demessence *et al.*[23] who obtained refractive indices of 1.23 and 1.18 for capillary and draining regime, respectively. The significantly higher n values ($>$1.54) reported in our work correspond to a much greater density, which can be associated with the absence of inter-grain porosity.

The relatively low standard deviations, determined from three spot measurements on a single film, of the film thickness (0.5%) and the refractive index (0.03%) at u_c indicate that intermediate withdrawal speeds allow for high film uniformity. At u_c, the standard deviations are an order of magnitude lower as compared to the other regimes. Within the 2 mm diameter spot size, no depolarization of the light is observed, implying low thickness non-uniformity.

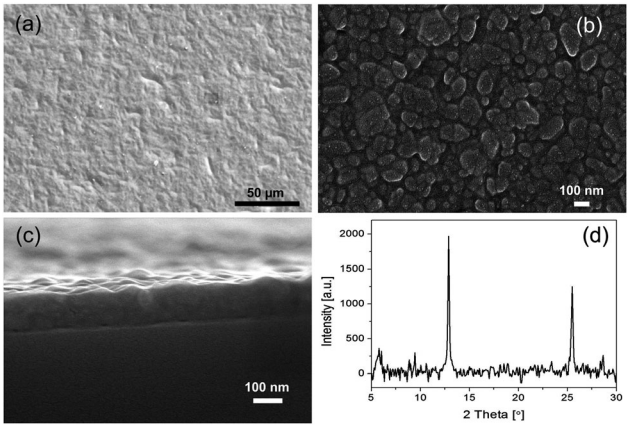

Fig. 2 Representative ZIF-8 nanofilm (u = 3 mm s^{-1}): (a) scanning electron microscope image of top view, (b) high magnification top view, and (c) cross section, (d) X-ray diffraction pattern.

These results indicate that intermediate withdrawal speeds favour the preparation of high-quality ultrathin uniform nanofilms. Very recently, Berteloot *et al.* reported continuous and relatively uniform silica nanofilms at u_c, as compared to the films synthesized at capillary and draining regimes.[29]

The uniformity of the films is also apparent from scanning electron microscope images (Fig. 2a–c). The film top view reveals no apparent cracks or pinholes. At higher magnification the top view reveals 10^{-7} m sized grains that do not exhibit distinct crystal characteristics such as sharp and well-defined edges normally observed for rhombic dodecahedral ZIF-8. The cross-sectional view of the film suggests that these grains are accommodated within a continuous film, without apparent grain boundary defects. X-Ray diffraction data prove that the films comprise ZIF-8 (Fig. 2d). The crystallites are oriented by the surface {112} parallel to the surface of the silicon substrate as is evidenced from the most intense peak positioned at 2theta = 12.8°. The films are likely to be bonded to the negatively charged native silica oxide layer *via* electrostatic interactions with the zinc ions. No delamination of the films during the exposure to vacuum, carbon dioxide, as well as during solvent rinse, was observed.

The non-crystalline characteristics of the films are apparent from the dynamics of the thickness and refractive index when exposed to vacuum, helium, and binary carbon dioxide–helium mixtures (Fig. 3). At the start of the dynamic *in situ* ellipsometry experiment, the value of n is lower as compared to that in Fig. 1, whereas the difference in film thickness is insignificant. During evacuation and subsequent exposure to 1 bar He a progressive decrease in n is observed. The concurrent change in thickness is only small. This means that remaining moieties, such as methanol, are removed from the film and empty void space is created inside the film. From the change in refractive index, the porosity can be estimated to be at least ~36% (ESI†). The rate of the slow process is accelerated by an increase in temperature from 35 °C to 70 °C. Subsequent incubation of the film at 70 °C reveals another long-term process, manifested by an increase in n and a constant thickness. The slow change in n is similar to that observed during physical aging of glassy organic polymers.[30] The non-equilibrium characteristics of such glassy materials induce a slow densification process.

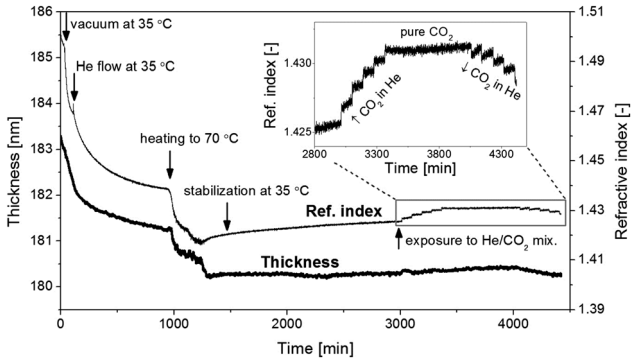

Fig. 3 *In situ* spectroscopic ellipsometry monitoring of a representative ZIF-8 nanofilm (u = 4 mm s^{-1}). Inset: changes in refractive index as a response to a stepwise introduction of CO_2; each step represents an additional 20 vol% increase in CO_2 concentration (for the amount of CO_2 sorbed see: ESI,† Fig. S2).

The constant thickness of the ZIF-8 films suggests that this material undergoes another morphological change than densification. This is supported by an increase of the gradient in density required for adequate optical fitting of the spectroscopic ellipsometry data. Upon exposure of the film to a mixture of 20 vol% carbon dioxide and 80 vol% He, a step change increase in the refractive index is observed, followed by progressively increasing n. The slope of n with time relates to the morphological rearrangement, which is slightly enhanced by the presence of the carbon dioxide. Upon subsequent further increase of the carbon dioxide concentration, a further increase in n is observed, while the morphological rearrangement becomes less pronounced. For exposure to pure carbon dioxide the rearrangement appears to be inhibited. Upon subsequent stepwise reduction of the carbon dioxide concentration, a stepwise reduction in refractive index is observed with an initially enhanced morphological rearrangement. The final value of n after the exposure cycle is higher than prior to the carbon dioxide exposure. The irreversible evolution of the refractive index indicates that the film is not entirely rigid and crystalline, but comprises nanoscale ZIF-8 crystals in a non-crystalline phase.

The high refractive indices of the films imply high film density. This indicates that the embedment of the nano-scale ZIF-8 crystals in the non-crystalline phase eliminates the presence of mesoporous inter-crystalline voids. Such inter-crystalline voids have dimensions that exceed those of small molecules, and dictate the dynamics and molecular selectivity of sorption and diffusion. Despite the overall high density, the films exhibit a high porosity (>36%) that is accessible to small molecules. The unprecedented homogenous continuous morphology, combined with the absence of inter-crystalline voids, provides distinct advantages in a variety of applications that rely on molecular distinction, for instance in membrane separations, adsorption, and chemical sensing.

The analysis of one year aged film showed a very similar dynamic response to pure CO_2, as compared to the response of freshly-synthesized nanofilms (ESI,† Fig. S3).

In summary, we have employed a step-by-step dip coating approach for the synthesis of uniform, dense, and defect-free ZIF-8 ultrathin nanofilms. The method enables accurate control of the final film thickness and density by the adjustment of the withdrawal speed. A critical withdrawal speed exists, at which films of a minimum thickness of 106 nm are obtained. At the critical withdrawal speed, the highest film uniformity is observed. The nanofilms exhibit comparatively high refractive indices, *ca.* 30% higher than compared to films presented in the literature. The high refractive indices are associated with the absence of mesoporous inter-particular voids. The films are partly crystalline. The non-crystalline characteristics are apparent from a long-term irreversible morphological rearrangement of the film, as is revealed by *in situ* spectroscopic ellipsometry. The high density of the films and SEM images suggest the absence of apparent mesoporous inter-crystalline voids, allowing for distinct molecular selective sorption and diffusion as compared to existing ZIF-8 films.

Notes and references

1 C. E. Wilmer, M. Leaf, C. Y. Lee, O. K. Farha, B. G. Hauser, J. T. Hupp and R. Q. Snurr, *Nat. Chem.*, 2012, **4**, 83–89.
2 H. Furukawa, K. E. Cordova, M. O'Keeffe and O. M. Yaghi, *Science*, 2013, **341**, 1230444.
3 J. Lee, O. K. Farha, J. Roberts, K. A. Scheidt, S. T. Nguyen and J. T. Hupp, *Chem. Soc. Rev.*, 2009, **38**, 1450.
4 O. Shekhah, J. Liu, R. A. Fischer and C. Wöll, *Chem. Soc. Rev.*, 2011, **40**, 1081.
5 K. Sumida, D. L. Rogow, J. A. Mason, T. M. McDonald, E. D. Bloch, Z. R. Herm, T.-H. Bae and J. R. Long, *Chem. Rev.*, 2012, **112**, 724–781.
6 D. Farrusseng, *Metal-Organic Frameworks*, John Wiley & Sons, 2011.
7 Y. Liu, E. Hu, E. A. Khan and Z. Lai, *J. Membr. Sci.*, 2010, **353**, 36–40.
8 K. S. Park, Z. Ni, A. P. Côté, J. Y. Choi, R. Huang, F. J. Uribe-Romo, H. K. Chae, M. O'Keeffe and O. M. Yaghi, *Proc. Natl. Acad. Sci. U. S. A.*, 2006, **103**, 10186–10191.
9 Y. Pan, Y. Liu, G. Zeng, L. Zhao and Z. Lai, *Chem. Commun.*, 2011, **47**, 2071.
10 H. Bux, C. Chmelik, R. Krishna and J. Caro, *J. Membr. Sci.*, 2011, **369**, 284–289.
11 H. Bux, F. Liang, Y. Li, J. Cravillon, M. Wiebcke and J. Caro, *J. Am. Chem. Soc.*, 2009, **131**, 16000–16001.
12 M. C. McCarthy, V. Varela-Guerrero, G. V. Barnett and H.-K. Jeong, *Langmuir*, 2010, **26**, 14636–14641.
13 R. Banerjee, A. Phan, B. Wang, C. Knobler, H. Furukawa, M. O'Keeffe and O. M. Yaghi, *Science*, 2008, **319**, 939–943.
14 B. Wang, A. P. Côté, H. Furukawa, M. O'Keeffe and O. M. Yaghi, *Nature*, 2008, **453**, 207–211.
15 C.-H. Kuo, Y. Tang, L.-Y. Chou, B. T. Sneed, C. N. Brodsky, Z. Zhao and C.-K. Tsung, *J. Am. Chem. Soc.*, 2012, **134**, 14345–14348.
16 A. A. Talin, A. Centrone, A. C. Ford, M. E. Foster, V. Stavila, P. Haney, R. A. Kinney, V. Szalai, F. El Gabaly, H. P. Yoon, F. Leonard and M. D. Allendorf, *Science*, 2014, **343**, 66–69.
17 P. Á. Szilágyi, R. J. Westerwaal, R. van de Krol, H. Geerlings and B. Dam, *J. Mater. Chem. C*, 2013, **1**, 8146.
18 R. Ameloot, F. Vermoortele, W. Vanhove, M. B. J. Roeffaers, B. F. Sels and D. E. De Vos, *Nat. Chem.*, 2011, **3**, 382–387.
19 D. Jiang, A. D. Burrows, Y. Xiong and K. J. Edler, *J. Mater. Chem. A*, 2013, **1**, 5497.
20 P. Horcajada, C. Serre, D. Grosso, C. Boissiere, S. Perruchas, C. Sanchez and G. Férey, *Adv. Mater.*, 2009, **21**, 1931–1935.
21 W.-J. Li, S.-Y. Gao, T.-F. Liu, L.-W. Han, Z.-J. Lin and R. Cao, *Langmuir*, 2013, **29**, 8657–8664.
22 G. Lu and J. T. Hupp, *J. Am. Chem. Soc.*, 2010, **132**, 7832–7833.
23 A. Demessence, C. Boissiere, D. Grosso, P. Horcajada, C. Serre, G. Férey, G. J. A. A. Soler-Illia and C. Sanchez, *J. Mater. Chem.*, 2010, **20**, 7676.
24 K. Kida, K. Fujita, T. Shimada, S. Tanaka and Y. Miyake, *Dalton Trans.*, 2013, **42**, 11128.
25 C. Hou, Q. Xu, J. Peng, Z. Ji and X. Hu, *ChemPhysChem*, 2012, **14**, 140–144.
26 O. Shekhah and M. Eddaoudi, *Chem. Commun.*, 2013, **49**, 10079.
27 L. Landau and B. Levich, *Acta Physicochim. URSS*, 1942, **17**, 42–54.
28 M. Faustini, B. Louis, P. A. Albouy, M. Kuemmel and D. Grosso, *J. Phys. Chem. C*, 2010, **114**, 7637–7645.
29 G. Berteloot, A. Daerr, F. Lequeux and L. Limat, *Chem. Eng. Process.*, 2013, **68**, 69–73.
30 L. Struik, *Physical aging in amorphous polymers and other materials*, Elsevier, Amsterdam, 1978.

